AIAA JOURNAL
Vol. 34, No. 2, February 1996

Ballistic Impact Response for Two-Step Braided Three-Dimensional Textile Composites

S. T. Jenq* and J. J. Mo†
National Cheng Kung University, Tainan, Taiwan 701, Republic of China

We are concerned with the ballistic impact response of three-dimensional two-step braided textile composites struck by a 36.1-g hemispherical tip-ended rigid cylindrical projectile. A series of quasistatic punch tests using a hemispherical indentor have been conducted to investigate the progressive damage modes of the target and to obtain the punch load-displacement relationship. In addition, a pneumatic launcher is used to propel the projectile with incident velocities ranging from 70 to 170 m/s. The ballistic limit is experimentally determined to be near 74.1 m/s. Commercially available finite element code (MARC) is incorporated with the constitutive relationship for three-dimensional two-step braided composites and the proposed static penetration model to simulate the dynamic impact response. An energy consideration is applied to predict the projectile's residual (or terminal) velocity. Numerical simulated result based on the static elastic properties of the target tends to overestimate the projectile terminal velocity. When the target's elastic moduli used in simulation are increased by 1.5 times the static values, good agreement is found between the simulated terminal velocities and test results for projectile incident velocities ranging from 70 to 180 m/s.

I. Introduction

POLYMER-MATRIX laminated composites have superior lightweight and sound mechanical properties and are extensively used in aerospace, automotive, and other related applications. Specially tailored laminates also exhibit rather good impact resistance and damage tolerance. An extensive summary of research related to damage in laminated composites due to low velocity impact can be found in Ref. 1. Methods for improving impact resistance of laminated composite structures have been investigated over the past two decades. In addition to adopting toughened matrix and/or fiber systems with an optimal lay-up, impact resistance can be further enhanced by innovations, such as through-the-thickness stitching, interleaving, weaving, and braiding. In recent years, interest in the development of textile preform reinforced composites has grown due to their unique mechanical properties.

Advancements in textile technology gave rise to novel methods of three-dimensional fiber reinforced braided textile preforms.[2] Typical research on the elastic stiffness, tensile modulus, and strength of three-dimensional braided composites is referred to by Byun and Chou,[3] Ko,[4] and Ma et al.[5] Textile composites with three-dimensional reinforced woven or braided preforms have been found to exhibit enhanced interlaminar surface characteristics, better through-thickness stiffness and strength, and improved damage tolerance. Using a drop tower impact tester, Ko and Hartman[6] found that braided composites possess a higher capacity for damage resistance than three-dimensional (XYZ) and two-dimensional (XY) orthogonally woven fabric composites. Gong and Sankar[7] used an instrumented impact pendulum and a projectile gas gun to study the impact response and related damage tolerance of three-dimensional braided graphite/epoxy composites. They reported that the braided composites show better damage tolerance than quasi-isotropic laminates with similar bending stiffness in the primary direction in both static and impact tests. The impact damage patterns and the factors that affect the extent and modes of impact damage were also examined experimentally.

When designing a suitable lightweight protective structure subjected to ballistic impact loading, it is important to understand the perforation condition (e.g., the ballistic limit) of composite structures in question. The ballistic limit is a critical projectile speed just sufficient to cause a complete penetration (CP). When the target is struck by an impactor traveling at an incident velocity equals to the ballistic limit, the projectile terminal (or residual) speed is zero. A more detailed description on the ballistic limit is referred to in Ref. 8. Since only scant research was found in which the penetration/perforation behavior of composite laminates was analytically modeled and the ballistic limit for laminated structures was predicted,[9-13] and since no published work was found on analytical modeling of penetration/perforation conditions to predict the terminal projectile velocity and the ballistic limit for three-dimensional reinforced braided textile composites, a series of impact tests are conducted in this work to study the penetration/perforation condition of three-dimensional two-step braided glass/epoxy textile composite targets struck by a 36.1-g hemispherical tip-ended rigid cylindrical penetrator. In a way similar to that used in ballistic impact modeling for graphite/epoxy and plain woven glass/epoxy laminates, reported by Lee and Sun[11,12] and Jenq et al.,[13] quasistatic punch tests are conducted to examine the punch load-displacement relationship and to characterize the penetration process for three-dimensional two-step braided textile composites. The quasistatic penetration model developed in this paper is then incorporated into the commercially available finite element code (MARC) as the penetration criteria to analyze the dynamic impact response. The constitutive relationship for three-dimensional two-step braided composites[3,14,15] and the modified Hertz contact law[16] are also used as the user-supplied subroutines in the finite element analysis. Energy balance consideration is adopted to predict the ballistic limit. Comparison between the predicted ballistic limit and that obtained from tests is reported. In addition, the test-determined and code-predicted projectile residual (or terminal) velocities after perforation are examined. Because of the rate-sensitive nature of glass/epoxy composites,[17-19] the effect of dynamic elastic moduli on the predicted projectile terminal velocity and ballistic limit is also studied numerically.

II. Experimental Setup and Test Results

A. Static Penetration Test and Result

The two-step braiding technique[2] is employed here to fabricate the three-dimensional fiber preform, and a vacuum assisted resin transfer modeling (RTM) method is used to manufacture the braided composite targets. Unidirectional E-glass fiber roving (Taiwan Glass Co. Ltd.) is used as the axial and braider yarns for the perform. The preform is then infiltrated with an epoxy resin system composed of Araldite LY564 and HY2954 (Ciba-Geigy). This resin system was designed for producing high-performance composite components

Received March 21, 1995; revision received Aug. 20, 1995; accepted for publication Aug. 24, 1995;

*Associate Professor, Institute of Aeronautics and Astronautics. Member AIAA.
†Graduate Assistant, Institute of Aeronautics and Astronautics.

Table 1 Basic mechanical properties of the epoxy matrix and the E-glass fiber yarns

	E-glass yarn	Epoxy matrix
Young's modulus E, GPa	72	2.6
Shear modulus G, GPa	29.5	0.963
Poisson's ratio ν	0.22	0.35
Density ρ, kg/m^3	2570	1150
Linear density λ, kg/m	0.0018	—

Table 2 Geometrical parameters of the two-step braided fiber perform

Braider pitch length h, m	0.01
Aspect ratio of axial yarn f_a	1
Aspect ratio of braider yarn f_b	5
Packing fraction of axial yarn κ_a	0.635
Packing fraction of braider yarn κ_b	0.635
Number of axial yarn along specimen's width direction m	13
Number of axial yarn along specimen's thickness direction n	2

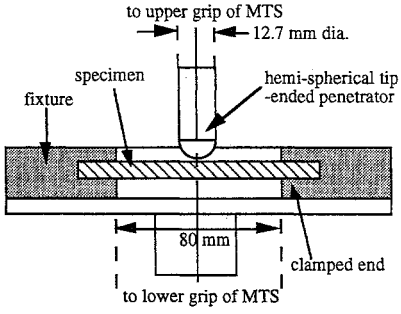

Fig. 1 Schematic drawing of the quasistatic punch test setup.

in conjunction with the RTM process. The weight ratio of epoxy (Araldite LY564) and hardener (HY2954) is approximately three to one. A mold release agent is applied to the mold surface to obtain a smooth specimen surface after cure. The specimen is then cured in an oven at 140°C for 7–8 h. Basic properties of the matrix and the yarns are listed in Table 1. The thickness and width of these rectangular braided composite specimens are 3.6 and 25.1 mm, respectively. The fiber volume fraction is about 0.45. Table 2 shows the geometrical parameters of E-glass fiber preform that are used to calculate the mechanical properties of the two-step braided specimen.

In the quasistatic test, the specimen is rigidly clamped along both ends with a span of 80 mm on an MTS tester (MTS System Corp., Minneapolis, MN). During the test, a hemispherical tip-ended cylindrical rigid penetrator with a length and diameter of 100 and 12.7 mm, respectively, is used, and the stroke rate of the penetrator is controlled at 0.125 mm/s. Figure 1 shows this quasistatic punch test setup. The purpose of performing these punch tests is to characterize the progressive damage mechanisms and to obtain the punch load-displacement curve to characterize the penetration process for dynamic analysis. Similar methods to predict the ballistic limit of graphite/epoxy laminate and plain woven glass/epoxy laminated composites were reported by Lee and Sun[11] and Jenq et al.,[13] respectively.

Three typical load-displacement curves measured from quasistatic punch tests are plotted in Fig. 2. It is noted that the test curves are reproducible and maintain a specific pattern. The basic pattern possesses physical meaning related to damage modes of braided composites due to quasistatic penetration by a hemispherical tip-ended rigid indentor, and it can be represented by the curve shown in Fig. 3. There are seven checkpoints (O, A, B, C, D, E, and F) marked in Fig. 3 for convenience. For a specimen loaded from point O to A, a nearly linear relationship between load and displacement is observed. No major damage mode is detected in tests with the exception of very tiny matrix cracks found in the area under contact. If the loading level is higher than that for checkpoint A, the

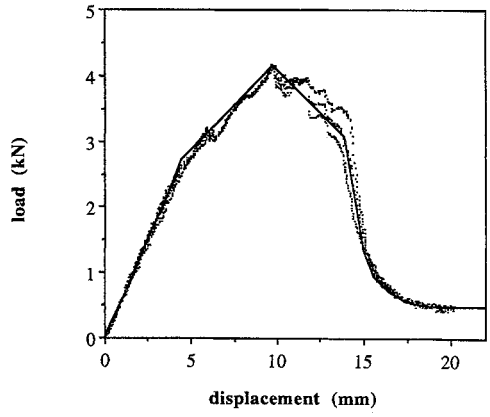

Fig. 2 Three typical load-displacement curves (dotted curves) measured from quasistatic punch tests and the numerical simulated curve (solid line).

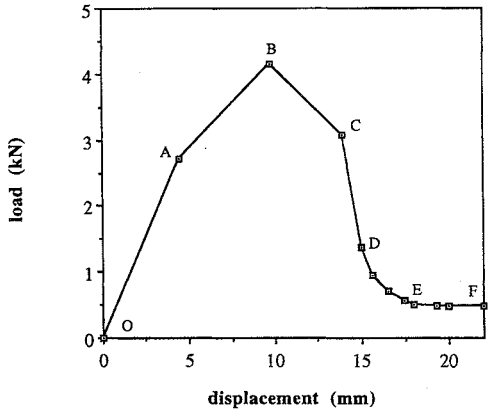

Fig. 3 Basic pattern of the quasistatic punch curves for two-step braided specimens studied.

slopes of the load-displacement curves shown in Fig. 2 decrease, and the matrix cracks start to propagate in the specimen. When the specimen is loaded along loading path BC, the fibers located close to the contact surface start to break progressively (in addition to matrix breakage), and this results in descending loads as the stroke of the penetrator increases. If this hemispherical indentor is further pressed downward, the damage area containing broken fibers continuously increases and results in extensive damage in the specimen. Therefore, the corresponding structural stiffness is further decreased in loading path CD. As the punch deeply penetrates into the target along loading path DE, the remaining intact fibers (containing both axial and braider yarns), located near the distal surface of the specimen, fracture and the broken fibers are pushed in the direction of penetrator motion out of the distal surface of the target. The current load-displacement pattern differs from that found in laminated composite specimens reported previously, and, as expected, no delamination phenomenon is observed. At checkpoint E, the tip of the penetrator almost exists from the distal surface of the target. A nearly constant frictional force between the penetrator and the target is observed at the loading path EF. Notice that if we compare the punch load-displacement curves shown in Fig. 2 and those reported by Lee and Sun[11] and Jenq et al.,[13] no abrupt loading decrease, representing the major delamination damage mode, is observed here. Furthermore, no obvious transition region for friction is observed since the plugging phenomenon does not prevail in the current study that uses a hemispherical penetrator. Photographs of an undamaged specimen and a quasistatically punched specimen are presented in Figs. 4a and 4b, respectively.

B. Dynamic Impact Test and Result

Eight high-speed impact tests are conducted to examine the impact damage of two-step braided textile composites and to determine the residual (or terminal) velocity and the ballistic limit of specimens

Table 3 Summary of dynamic impact test results

Test no.	Incident velocity V_s, m/s	Exit velocity V_r, m/s	Estimated ballistic limit, m/s	Change of energy,[a] kg^2/s^2	Change of momentum,[b] kg/s	Note[c]
D1	70.5	—	—	—	—	PP with rebound
D2	74.1	0	74.1	99.1	2.68	CP and stuck on target
D3	79.6	11.3	78.8	112.1	2.47	CP
D4	99.6	53.3	84.1	127.8	1.67	CP
D5	110.5	66.4	88.3	140.8	1.59	CP
D6	114.9	73.8	88.1	140.0	1.48	CP
D7	132.2	95.3	91.6	151.5	1.33	CP
D8	165.0	130.0	101.6	186.4	1.26	CP

[a]The change of projectile's kinetic energy is equivalent to $[\frac{1}{2}(m_p)(V_s^2 - V_r^2)]$.
[b]The change of projectile's momentum is equivalent to $[m_p(V_s - V_r)]$.
[c]PP represents partial penetration; CP represents complete penetration.

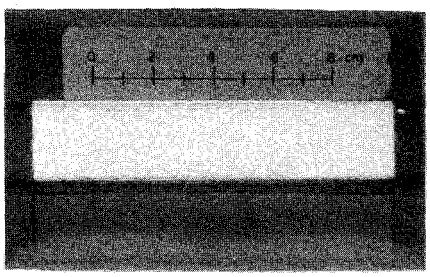

a) Top view of undamaged specimen

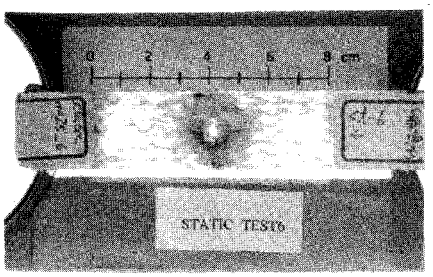

b) Top view

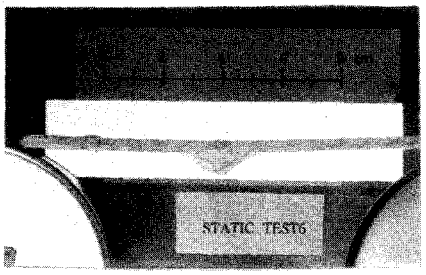

Side view

Fig. 4 Photographs for a) undamaged specimen and b) quasistatically punched specimen.

struck by a hemispherical tip-ended cylindrical rigid projectile with a length of 38.7 mm and weighing 36.1 g. The diameter of the penetrator is 12.7 mm, which is same as the diameter of the indentor used in quasistatic punch tests. A pneumatic gun is used to propel the projectile against targets with incident velocities ranging from 70 to 170 m/s. The ballistic limit is experimentally determined to be near 74.1 m/s. The projectile incident and terminal velocities are detected by a pair of photosensors and a set of short screens, respectively. A schematic drawing of the dynamic impact test system is referred to in a previously published paper.[13] The major damage patterns found in the impacted specimens are indentation, matrix cracking (including resin pocket matrix damage), breaking of axial and braider fiber yarns, and broken fibers pulled outward. Figures 5a–5d show photographs of the selected impact damaged specimens when the projectile is fired at a velocity of 74.1, 99.6, 132.2, and 165 m/s, respectively. These damage patterns are similar to those found in the quasistatic penetrated spacimens. The dynamic impact damaged area is close to that found in quasistatic tests if the projectile incident velocity is approximately less than 110 m/s. However, in higher impact velocities ranging from 110 to 170 m/s, the impact damaged zone extends outward considerably, as shown in Figs. 5c and 5d.

Using the test results, the estimated ballistic limit shown in the fourth column of Table 3 is calculated based on the principle of conservation of energy for a rigid penetrator to satisfy the following simple relationship[8,12]:

$$\tfrac{1}{2}m_p V_{BL}^2 = \tfrac{1}{2}m_p V_s^2 - \tfrac{1}{2}m_p V_r^2 \qquad \text{for} \qquad V_s > V_{BL} \qquad (1)$$

where m_p is the mass of the projectile, and the estimated ballistic limit is represented by V_{BL}. The striking velocity and residual velocity of the projectile are denoted by V_s and V_r, respectively. An examination of the estimated ballistic limit listed in Table 3 reveals that the average estimated ballistic limit is 79 m/s for test number D2, D3, and D4. This value is close to the test-determined ballistic limit of 74.1 m/s. However, the estimated value increases as the incident velocity is increased. This discrepancy seems to result from the fact that the damage region is increased when the target is impacted by a projectile at an incident velocity that is higher than 110 m/s. Notice that the kinetic energy absorbed by two-step braided composite targets also increases in higher impact velocity tests (e.g., test D5 to D8), as shown in the fifth column of Table 3.

III. Predicting Elastic Moduli for Two-Step Braided Targets

The yarn cross sections of two-step braided rectangular specimens after adding matrix and consolidation can be assumed to be flattened[14] as shown in Fig. 6. The axial yarn cross section is dependent on its location in the fabric, shown as the darkened area in Fig. 6 for a [12, 4] braided structure. Here $[m, n]$ notation is used to describe the arrangement of m columns by n rows of axial yarns located in the cross-sectional boundary of a braid, and the axial and thickness directions of the sample are plotted along x and z axis, respectively.[2] To simplify the modeling process for computing a target's elastic moduli for subsequent finite element analysis, the cross

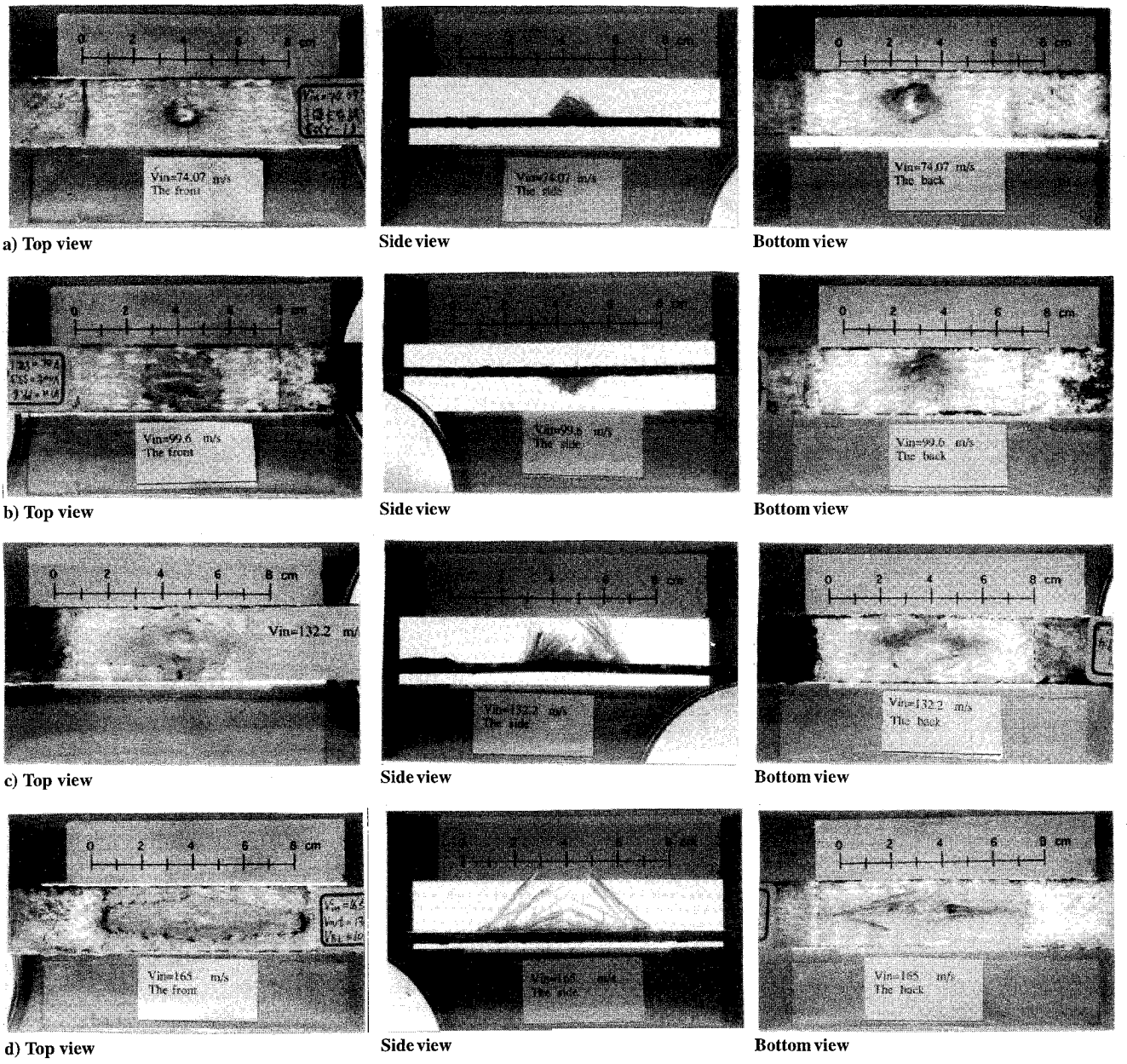

Fig. 5 Photographs of dynamic impact damaged specimens struck by a hemispherical projectile at the velocity of a) 74.1, b) 99.6, c) 132.2, and d) 165 m/s.

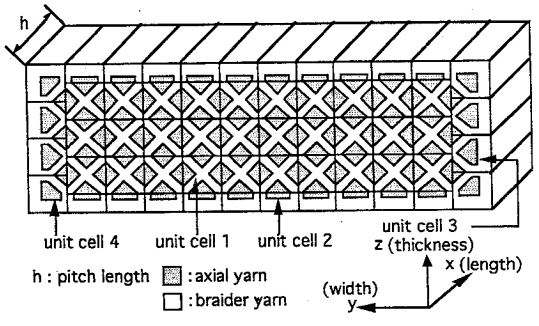

Fig. 6 Cross section of the [12, 4] braided specimen.[15]

sections can be divided into four unit cells (i.e., unit cells 1–4 shown in Fig. 6). Braided rectangular plate specimens [13, 2] are used in the current applications. The corresponding yarn cross-sectional view and a drawing of axial and braider yarns on the surface parallel to the x–y plane are presented in Figs. 7a and 7b, respectively. Notice that only three types of unit cells occur in the present study. Figure 8 shows the axial yarn cross-sectional geometry relationship[15] (i.e., types I–IV) in the previously mentioned four unit cells. Consider type I shown in Fig. 8, and let the aspect ratio f_a of this cross section be defined as

$$f_a = (A/A') = \tan(\phi/2) \tag{2}$$

where subscript a represents the axial yarn, and the angle ϕ and length A and A' are the geometrical parameters shown in Fig. 8. In the present application, f_a is assumed to be unity. Therefore, length A is equivalent to that of A' and the angle $(\phi/2)$ is 45 deg. For an arbitrary fiber yarn, the net cross-sectional area (i.e., $A_{y\text{-net}}$ without including the gap between fibers) of yarn is equivalent to its linear density λ divided by density ρ. The cross-sectional area of fiber yarn with gap (i.e., $A_{y\text{-full}}$) can be written as

$$A_{y\text{-full}} = \left(\frac{A_{y\text{-net}}}{\kappa}\right) = \frac{\lambda}{\rho\kappa} \tag{3}$$

where κ is the packing fraction. Therefore, the cross section containing the fiber and gap for type I axial yarn is

$$A_{y\text{-full-type I}} = \lambda_a/\rho_a\kappa_a \tag{4}$$

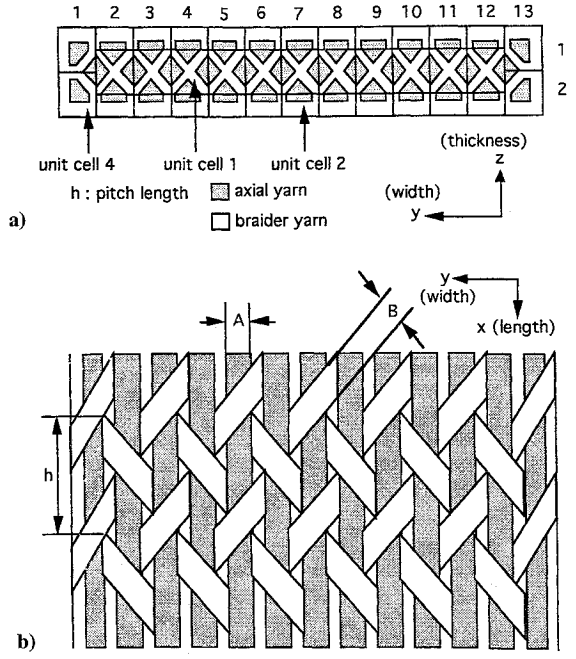

Fig. 7 a) Cross section of the [13, 2] braided specimen used in this work and b) arrangement of axial and braider yarns on the surface parallel to the x–y plane.

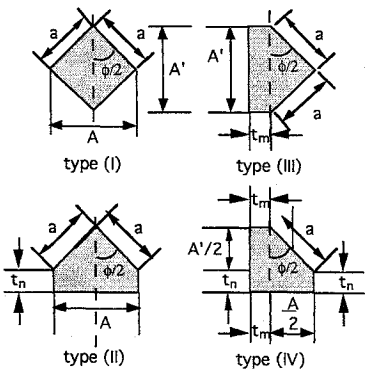

Fig. 8 Four types of cross sections containing axial yarn in unit cells 1–4, in a $[m, n]$ = [12, 4] braided specimen.[15]

Based on the geometrical relationship of the cross section of type I shown in Fig. 8, we know that

$$A_{y\text{-full-type I}} = a^2 \sin(\phi) \tag{5}$$

Equations (2), (4), and (5) yield

$$a = \sqrt{\frac{\lambda_a}{\rho_a \kappa_a \sin(\phi)}} = \sqrt{\frac{\lambda_a\left(1 + f_a^2\right)}{2\rho_a \kappa_a f_a}} \tag{6}$$

Similarly, the geometrical parameters t_m and t_n in Fig. 8 can be derived as

$$t_m = \frac{a}{2}\sin\left(\frac{\phi}{2}\right) = \frac{1}{2}\sqrt{\frac{\lambda_a\left(1 + f_a^2\right)}{2\rho_a \kappa_a f_a}}\frac{1}{\sqrt{1 + f_a^2}} = \frac{1}{2}\sqrt{\frac{\lambda_a f_a}{2\rho_a \kappa_a}} \tag{7a}$$

and

$$t_m = \frac{a}{2}\cos\left(\frac{\phi}{2}\right) = \frac{1}{2}\sqrt{\frac{\lambda_a\left(1 + f_a^2\right)}{2\rho_a \kappa_a f_a}}\frac{1}{\sqrt{1 + f_a^2}} = \frac{1}{2}\sqrt{\frac{\lambda_a}{2\rho_a \kappa_a f_a}} \tag{7b}$$

After substituting the given basic parameters listed in Tables 1 and 2 into Eqs. (7a) and (7b), both t_m and t_n are calculated to be 0.37×10^{-4} m for the specimen studied. In addition, the length A can also be expressed as

$$A = 4t_m = \sqrt{\frac{2\lambda_a f_a}{\rho_a \kappa_a}} \quad \text{and} \quad A' = 4t_n \tag{8}$$

Following the example set by Chou,[15] the cross section for braider yarn is assumed to be rectangular in shape. The aspect ratio f_b of braider yarn is similarly defined as

$$f_b = (B/b) \tag{9}$$

where subscript b represents braider yarn. Parameters B and b stand for the length and width of the rectangular cross-sectional area of braider yarns and satisfy the following relations:

$$b = \sqrt{\frac{\lambda_b}{\rho_b \kappa_b f_b}} \tag{10}$$

Based on preceding relationships, the resulting specimen's total width W and thickness T can be expressed as

$$\begin{aligned} W &= A\left(m - \tfrac{1}{2}\right) + (B/f_b)(m + 1) \\ T &= (A/f_a)\left(n - \tfrac{1}{2}\right) + (B/f_b)(n + 1) \end{aligned} \tag{11}$$

Note that m and n shown in the preceding equations have been defined earlier. The width W and thickness T of the specimen studied here are computed to be 25.08×10^{-3} and 3.63×10^{-3} m, respectively, and the corresponding measured data are 25.4×10^{-3} and 3.6×10^{-3} m, respectively. The difference is small.

The pitch length h, shown in Fig. 7b, is defined by a two-step movement of braider that constitutes a cycle when we fabricate the preform. Figure 9 shows the projection of a complete two-step movement of 30 braiding yarns on the y–z plane. If we consider a movement (e.g., 26-11-22) in Fig. 9, the length of braider yarns (L_1) projected onto the y–z plane in two steps of braiding (i.e., a single pitch length movement) can be determined as

$$L_1 = 4[2t_m + b + t_n + (b/2) + a + (b/2)] \tag{12}$$

Knowing the pitch length h and projected length of braider yarn L_1, the corresponding inclination angle θ_{L1} of braider fiber is then equivalent to $\tan^{-1}(L_1/h)$. Note that the inclined angles (i.e., θ_1 and θ_2) in unit cells 1 and 2 are modeled to be identical to θ_{L1}. Similarly, if we consider another complete two-step movement (e.g., 4-3-30) for braiding yarns related to unit cell 4 shown in Fig. 9. The projected length of braider yarn L_4 on the y–z plane is

$$L_4 = 4.5t_m + 4t_n + a + 4b \tag{13}$$

The corresponding inclination angle θ_4 for braided fiber in unit cell 4 can also be computed from $\theta_4 = \tan^{-1}(L_4/h)$. The fiber volume

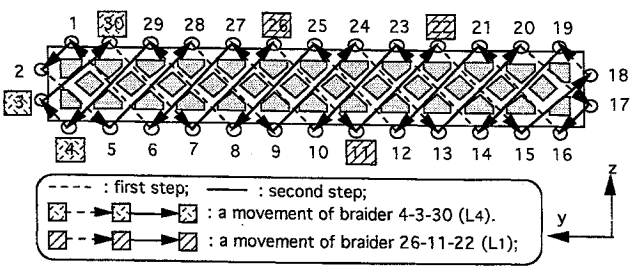

Fig. 9 Projection of the two-step movement of braider yarns on the y–z plane.

for unit cells 1, 2, and 4 (i.e., V_1, V_2, and V_4) containing both axial and braider yarns can finally be derived as

$$V_1 = 2h\left(\frac{\lambda_a}{\rho_a}\right) + \frac{\lambda_b}{\rho_b}\left(2\frac{2a+b}{\sin\theta_1} + \frac{b}{\sin\theta_1}\right)$$

$$V_2 = \frac{1}{2}h\left(\frac{\lambda_a}{\rho_a}\right) + \frac{\lambda_b}{\rho_b}\left(\frac{2t_n + 4t_m + 2b}{\sin\theta_2}\right) \qquad (14)$$

$$V_2 = \frac{5}{4}h\left(\frac{\lambda_a}{\rho_a}\right) + \frac{\lambda_b}{\rho_b}\left(\frac{4t_m + 4t_m + a + b}{\sin\theta_4}\right)$$

Then the fiber volume fraction for this two-step braided composite, with $[m, n]$ equivalent to [13, 2], can be written as

$$V_f = \frac{(11V_1 + 22V_2 + 4V_4)}{TWh} \qquad (15)$$

Based on the prescribed data given in Tables 1 and 2, the computed fiber volume fraction V_f of the sample is calculated to be 0.45, which equals the test-determined value.

Elastic properties in each unit cell of two-step braided composites can be predicted based on the fiber and matrix properties and the three-dimensional fiber architecture.[14,15] It is assumed that axial and braider yarns are considered to be unidirectional composite cylinders after resin impregnation. Because the principal material directions of the three-dimensional braider yarns do not coincide with the global x-y-z coordinate directions of the plate-type specimen, a coordinate transformation from one inclined coordinate system to another is needed. The material coordinate system is represented by the 1-2-3 system is usual, where axis 1 coincides with the yarn's axial direction. The x axis of the global coordinate system is along the composite longitudinal direction, and y and z axes are in the width and thickness directions of composites. An arbitrary θ angle of braider yarn is used to represent inclination with respect to the x axis; θ_x is the angle of the projected yarn on the x–y plane with respect to the x axis; and θ_z is the yarn angle measured from the x–y plane, respectively. Because of the transverse isotropy, the compliance matrix $[S]_{scc}$ of the single composite cylinder in the 1-2-3 coordinate system can be expressed as

$$[S]_{scc} = \begin{bmatrix} 1/E_{11} & -\nu_{21}/E_{22} & -\nu_{21}/E_{22} & 0 & 0 & 0 \\ -\nu_{21}/E_{11} & 1/E_{22} & -\nu_{32}/E_{22} & 0 & 0 & 0 \\ -\nu_{12}/E_{11} & -\nu_{23}/E_{22} & 1/E_{22} & 0 & 0 & 0 \\ 0 & 0 & 0 & 1/G_{23} & 0 & 0 \\ 0 & 0 & 0 & 0 & 1/G_{12} & 0 \\ 0 & 0 & 0 & 0 & 0 & 1/G_{12} \end{bmatrix} \qquad (16)$$

where E_{ij}, G_{ij}, and ν_{ij} represent the Young's modulus, shear modulus, and Poisson's ratio, respectively. These unidirectional cylinder properties are obtained from the fiber and matrix properties using micromechanics analysis. Then the compliance matrix of a unidirectional composite cylinder, referring to the 1-2-3 coordinate system, is transformed to $[S^*]$, referring to the x-y-z system for inclined yarn:

$$[S^*] = [T]^t[S][T] \qquad (17)$$

where $[T]$ is the coordinate transformation matrix. If we assume that the 2 axis of braider yarn is perpendicular to the z axis, the direction cosines (α_i, β_j, and γ_k, where indices i, j, and k = 1, 2, or 3) in the transformation matrix $[T]$ can be expressed as[2]

$$\begin{aligned} \alpha_1 &= \cos\theta_x\cos\theta_z; & \alpha_2 &= \sin\theta_x\cos\theta_z; & \alpha_3 &= \sin\theta_z \\ \beta_1 &= \sin\theta_x; & \beta_2 &= \cos\theta_x; & \beta_3 &= 0 \\ \gamma_1 &= -\cos\theta_x\sin\theta_z; & \gamma_2 &= -\sin\theta_x\sin\theta_z; & \gamma_3 &= \cos\theta_z \end{aligned} \qquad (18)$$

Table 4 Computed elastic moduli for unit cells 1, 2, and 4 in a [13, 2] two-step braided composite

	Computed elastic moduli		
	Unit cell 1	Unit cell 2	Unit cell 4
E_{xx}, GPa	20.05	13.67	19.87
E_{yy}, GPa	6.93	7.23	7.10
E_{zz}, GPa	6.93	6.88	7.10
ν_{xy}	0.31	0.35	0.35
ν_{yz}	0.33	0.25	0.27
ν_{zx}	0.11	0.16	0.13
G_{xy}, GPa	2.93	3.06	3.33
G_{yz}, GPa	3.02	2.24	2.17
G_{zx}, GPa	2.93	2.71	3.33

According to the geometrical relationship,[15,20] θ_x and θ_z can be expressed as $\tan^{-1}[f_a\tan\theta_i/(1+f_a^2)^{0.5}]$ and $\cos^{-1}[(\cos^2\theta_i+f_a^2)/(1+f_a^2)]^{0.5}$, respectively, and index i is equal to 1, 2, and 4 corresponding to unit cells 1, 2, and 4. The compliance matrix for axial and braider yarn (i.e., $[S]_a$ and $[S]_b$) can simply be written, respectively, as

$$[S]_a = [S]_{scc} \quad \text{and} \quad [S]_b = [T]^t[S]_{scc}[T] \qquad (19)$$

In addition, and global system compliance matrix ($[S]_m$) for assumed homogeneous and isotropic matrix material can be obtained simply. The average stiffness matrix method used by Byun and Chou[3] and Chou[15] is then adopted to predict the elastic properties for the [13, 2] two-step braided composite. The average stiffness matrix for unit cell i (i = 1, 2, or 4) can be obtained as

$$[\bar{C}]_i = (1/V_{ci})\{V_{ai}[C]_a + V_{bi}[C]_{bi} + V_{mi}[C]_m\} \qquad (20)$$

Stiffness matrices $[C]_a$, $[C]_b$, and $[C]_m$ are used to stand for the inverted compliance matrices of $[S]_a$, $[S]_b$, and $[S]_m$. Note that V_{ci}, V_{ai}, and V_{bi} represent the total volume, axial yarn volume, and braider yarn volume of the ith unit cell, respectively. The matrix volume V_{mi} for the ith cell is equivalent to (V_{ci}-V_{ai}-V_{bi}). Using the data given in Tables 1 and 2, which provide the geometrical and basic material parameters for current analysis, the computed elastic properties for unit cells 1, 2, and 4 are presented in Table 4. The difference between test-determined apparent axial elastic modulus and the model predicted value, based on those computed elastic moduli for unit cells 1, 2, and 4 and their corresponding volume ratios, is within 15%. This discrepancy may result from the fact that 1) during the braiding process, some fiber yarns are damaged and 2) current simplified modeling slightly deviates from the real specimen's geometrical relationship.

IV. Static and Dynamic Simulation Results and Discussion

The ballistic limit of two-step braided textile composite specimens is numerically computed to check against the test-determined result. As a continuation of previous work reported by Lee and Sun[11,12] and Jenq et al.,[13] the computational procedure for predicting the ballistic limit of two-step braided textile composite targets basically consists of four phases: 1) determine the penetration criterion based on the quasistatic punch curves obtained from tests to characterize the major damage mechanisms (containing matrix cracking and axial and braider yarns failure and pullout) and locate the termination of these mechanisms; 2) analytically model the elastic properties of two-step braided composite based on axial and braider fibers and matrix material properties and the geometrical relationship for braided composites; 3) apply finite element code (MARC) to take into account for the structural stiffness degradation to fit the quasistatic punch (load-displacement) curves; and 4) simulate the dynamic impact test conditions with the proposed static penetration model to determine the velocity of the hemispherical, tip-ended rigid impactor when major damage mechanisms have terminated. The modified Hertz contact law[16]

$$F = K\alpha^{\frac{3}{2}} \quad \text{and} \quad K = \frac{4}{3}R_S^{\frac{1}{2}}\left[\frac{1-\nu_S^2}{E_S} + \frac{1}{E_t}\right]^{-1} \qquad (21)$$

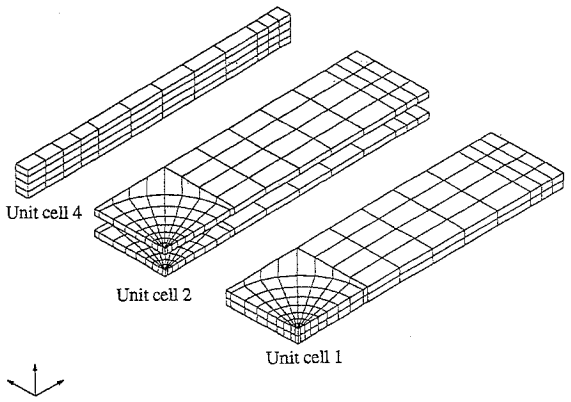

Fig. 10 Three-dimensional drawing of 432 elements, composed of unit cells 1, 2, and 4, in a quarter of the targets for finite element analysis.

is used to model the contact force F exerted on the two-step braided composite target and penetrator with a specific incident velocity. Parameter α represents the indentation and K is a constant that depends upon the projectile's tip radius R_S, the elastic modulus E_S, and the Poisson ratio ν_S of the penetrator, and the transverse elastic modulus E_t of the target in contact with the impactor. An anisotropic elastic relation that provides stiffness degradation for each unit cell of braided textile composite corresponding to proposed penetration criteria and the mentioned modified Hertz contact law are both utilized in the MARC finite element analysis as the user-supplied subroutines. Friction is not incorporated into finite element analysis, but an energy balance consideration is used to account for the frictional resistance to determine the projectile's residual (or terminal) velocity for complete perforation. The ballistic limit can then be subsequently calculated by using Eq. (1) for a given incident and the corresponding computed residual velocities. The impact response of a simply supported $20 \times 20 \times 0.8$-cm steel plate due to the central impact of a 2-cm-diam steel sphere at an initial velocity of 100 cm/s was numerically simulated using the MARC finite element code with an isotropic constitutive relationship to check against the analytical result reported by Karas (shown on page 140 of Ref. 21). Close agreement was found, but the results are not presented here.

Before performing the transient analysis of the two-step braided textile composite target struck by a hemispherical tip-ended projectile, static analysis using MARC finite element code was performed to simulate the quasistatic punch test conditions. A total of 432 element were employed for the quarter composite plate (due to symmetry) in the numerical analysis, as shown in Fig. 10. Specimen elements were characterized by three different sets of material properties (shown in Table 4) corresponding to unit cells 1, 2, and 4 to account for the unique architecture of the two-step braided specimen studied. Note that the 8-node isoparametric element (element type 7 of MARC program) was used. The numerical simulated static punch curve is presented in Fig. 2 as the solid curve, and test findings and simulated results are in good agreement. Initially, the specimen was loaded from checkpoint O to A as shown in Fig. 3. No damage was considered on loading path OA during numerical simulation. When loading level reached checkpoint A, both the Young's modulus and the shear elastic property of matrix material were degraded proportionally so that the simulated loading path is very close to the test curve in this range (loading path AB). Parameter r_m ($0 \leq r_m \leq 1$) was used to represent the extent of degradation for matrix material. The degraded properties E_m^* and G_m^* were set to be equivalent to $r_m E_m$ and $r_m G_m$, respectively. Note that E_m and G_m are the elastic properties of the matrix material before degradation. In loading path AB, the fiber degradation parameter r_f is set to be unity since almost no fiber breakage was observed in tests and the matrix material is degraded gradually to satisfy the loading path AB shown in Fig. 3. At checkpoint B, elastic moduli of matrix material are degraded to 17% of the original value (i.e., $r_m = 0.17$) for unit cells 1 and 2. In addition, the matrix elastic moduli of unit cell 4 are degraded to 58.5% of the original value ($r_m = 0.585$) since the matrix damage is less in unit cell 4 than in unit cells 1 and 2. According to the extent of damage observed

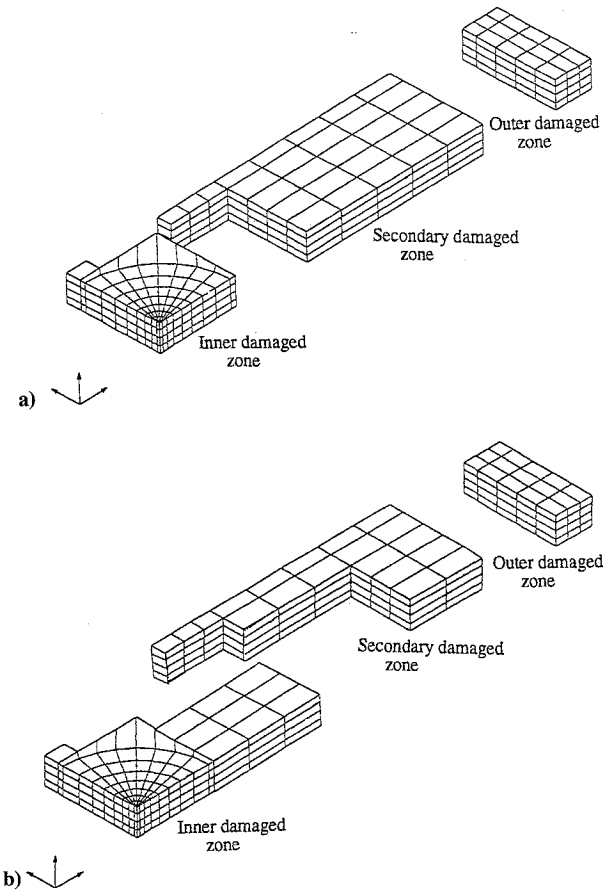

Fig. 11 Three-dimensional drawings of inner, secondary, and outer damaged zone in a quarter of the specimen plates for dynamic impact analysis when the incident velocity was a) less than 110 m/s and b) higher than 110 m/s.

in test samples, specimens are divided into 1) the inner damaged region, 2) the secondary damaged region, and 3) the outer damaged region, as shown in Fig. 11a. For loading path BC, both matrix and fiber degradation parameters r_m and r_f are further decreased in the inner damage region to account for the serious damage found around the region near impact to satisfy the test-determined result. At checkpoint C, degradation parameters r_m and r_f are simulated to be 0.1 in this region. The matrix and fiber degradation parameters in the secondary damage region are modeled to be the same as that for checkpoint B, whereas the corresponding fiber degradation parameters for the outer damaged region corresponding to checkpoint C is determined to be $r_f = 97.5\%$. When the sample was further loaded from checkpoint C to D, the matrix and fiber degradation parameters were determined to be 0.5% in the inner damaged zone. The corresponding degradation parameters for secondary and outer damaged zones in this loading path are set to be the same as those found for checkpoint C. Finally, in the DE loading path, only the matrix and fiber are further degraded to be 0.05% of the intact specimen's elastic moduli in the inner damaged zone. This means that the specimen is almost perforated by the impactor. The corresponding degradation values for the second and outer damaged zone are set to be the same as those at checkpoint E to account for the small amount of damage during impact. Figure 11b shows the extended major damage zone, the secondary damaged zone, and the outer damaged zone used for numerical analysis when impact velocity was higher than 110 m/s to account for the enlarged damaged pattern found in dynamic impact tests. A plot of the simulated fiber degradation parameters r_f for inner, secondary, and outer damaged zones vs displacement is presented in Fig. 12a. In addition, plots of the degradation factor r_m for the inner damaged zone and the secondary and outer damaged zones vs displacement are also presented in Figs. 12b and 12c, respectively. After checkpoint E, the projectile started to exit from the distal surface of the target, and a nearly

Table 5 Summary of the simulated impact test results

Run no.	Incident velocity, m/s	Simulated residual velocity,[a] m/s	Predicted ballistic limit,[b] m/s	Note
s1	70	12.53	68.87	The static elastic properties were used in the numerical simulations.
s2	80	32.3	73.2	
s3	100	59.5	80.4	
s4	130	96.7	86.9	
s5	150	120.6	89.19	
s6	180	154.77	91.91	
ds1	75	(Rebound)	—	The dynamic elastic properties were used in the numerical simulations.
ds2	80	14.65	78.6	
ds3	100	49.4	86.9	
ds4	130	86.5	97.0	
ds5	150	110.47	101.47	
ds6	180	145.5	105.97	

[a]The simulated residual velocity is computed based on Eq. (22).
[b]The predicted ballistic limit is calculated based on Eq. (1) for the given incident velocity and the residual velocity.

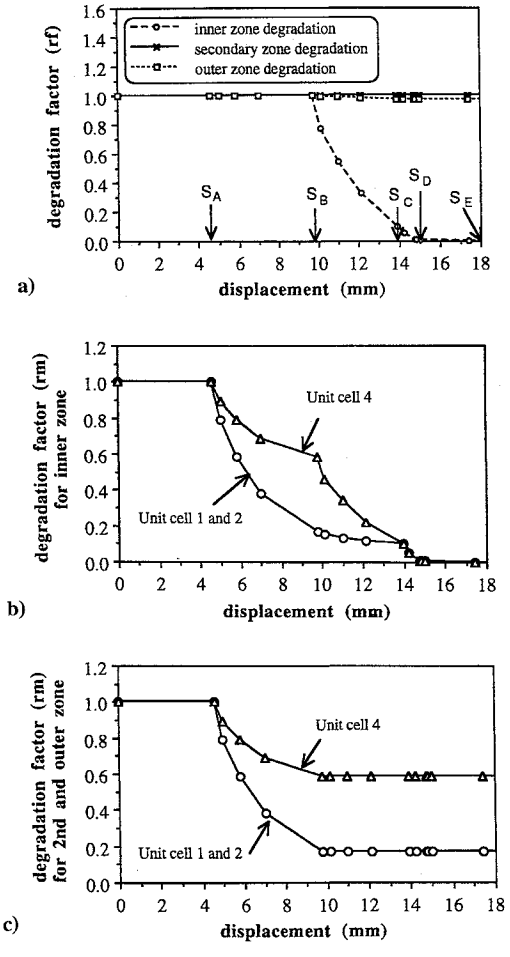

Fig. 12 Plot of the simulated degradation factor for a) fiber (r_f), b) matrix (r_m) in the inner damaged zone, and c) matrix (r_m) in the secondary and outer damaged zones.

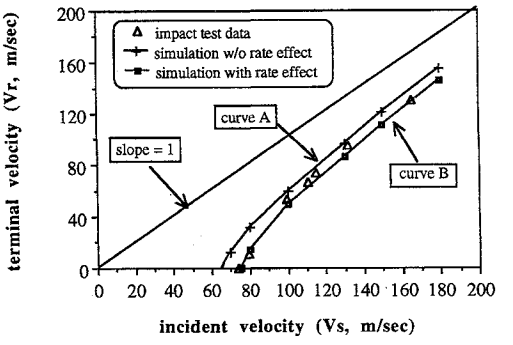

Fig. 13 Plot of the striking velocity (Vs) vs terminal velocity.

constant friction force is observed in the punch test curves. Aforementioned procedures are proposed to serve as guidelines for subsequent impact dynamic analysis, and the validity is to be justified by the agreement between experimental findings and the simulated results.

The transient analysis of the impact system was then numerically analyzed. Initially, the incident velocity of the projectile was specified and the target was assumed to be stress free and stationary. The simple displacement criteria were proposed to characterize the impact damage process. 1) When the displacement of impactor was loaded to check point A (i.e., $S_A = 4.59$ mm), shown in the static punch curve, the elastic moduli of the matrix in the inner, secondary, and outer damaged region of braided specimens were degraded to the values determined from the fitted results (Figs. 12a–12c) of the static punch simulation described in the preceding paragraph. 2) At checkpoint B (i.e., $S_B = 9.75$ mm), the fibers in the specimen started to break. When the target was further loaded along loading paths CD and DE, the elastic moduli of fiber and matrix for these three damaged regions were continuously degraded according to the fitted results obtained from the static punch simulation to account for the extensive damage mechanisms containing both matrix and fiber breakage. Note that the corresponding displacements (i.e., S_C and S_D) for checkpoint C and D are 13.93 and 15.0 mm, respectively, as shown in Fig. 12a. 3) When the specimen was continuously loaded to a displacement level (i.e., $S_E = 18.0$ mm) corresponding to checkpoint E, the specimen was on the verge of perforation and the finite element simulation was terminated.

The computed final velocity of the projectile, corresponding to checkpoint E, was then used to calculate the residual velocity V_r of projectile based on energy balance consideration

$$E_r = \tfrac{1}{2}m_p V_r^2 = \tfrac{1}{2}m_p V_E^2 - F_E b \tag{22}$$

where b represents the length of the projectile, and V_E and F_E are the projectile velocity and the steady friction force corresponding to checkpoint E and the frictional loading path beyond point E, respectively. By substituting the projectile residual velocity V_r from Eq. (2) into Eq. (1) for the specific incident velocity V_s, the predicted ballistic limit V_{BL} can be calculated correspondingly.

A series of impact test simulations (run nos. s1–s6) are performed for projectiles striking with a velocity ranging from 70 to 180 m/s. Note that the static elastic properties for unit cells 1, 2, and 4 shown in Table 4 are used as the input data. The predicted ballistic limit (shown in Table 5) increases as the incident velocity of the impactor increases, since the major impact damaged zone increases under higher impact velocity conditions. This trend is similar to that found in results from impact tests shown in Table 3. Figure 13 shows a plot of projectile incident velocity V_S vs terminal velocity V_r. At an incident velocity of 70 m/s, the simulated terminal velocity was 12.53 m/s, and this means that the target was perforated. Curve A in Fig. 13 corresponds to those simulations utilizing static elastic

properties. This curve intersects with the x axis (i.e., zero terminal velocity) at an incident velocity near 65 m/s, which is below the test-determined ballistic limit of 74.1 m/s. In addition, if we compare the triangular points that represent test results with curve A in Fig. 13, the simulated results seem to overestimate the projectile terminal velocity. This discrepancy may be due to the following reasons: 1) the proposed static penetration model for two-step braided composites incorporated in the transient finite element analysis is unable to closely predict the dynamic impact response and 2) the high strain-rate effect[17–19] on the variation of the dynamic elastic properties of glass/epoxy braided structures must be considered in numerical simulations.

A previous research paper[13] for predicting the ballistic limit for glass/epoxy plain woven laminated targets showed that the simulated projectile residual velocity and the corresponding ballistic limit become closer to those found in experiments when the dynamic elastic moduli (chosen to be two times the static values) are used as the input data in finite element analysis. Therefore, additional simulations (run nos. ds1–ds6) were performed using dynamic elastic moduli in the input data file to incorporate high strain-rate effects on the target due to impact. In the current application, the dynamic elastic moduli were chosen to be 1.5 times those of static values. The reasons for using this approximated factor of 1.5 are that 1) the fiber volume ratio of the present braided specimen is about 45%, which is less than the previously reported[18] high strain-rate data for specimens with fiber volume ratio of about 60% and 2) the axial fiber volume is approximately 50% of the total fibers in the specimen (the rest of the fibers are braider yarns). Note that an important topic is the determination of an accurate factor to account for the strain-rate effect of braided GFRP composite targets transversely struck by a projectile at the impact rate of strain. The corresponding simulated terminal velocity and the predicted ballistic limit using the dynamic elastic modulus degraded in the same trend as that used for runs s1–s6, as shown in Table 5. Based on the corresponding simulated results shown in this table, the ballistic limit should be close to 75 m/s, which is quite close to experimental results (i.e., 74.1 m/s). This can be observed clearly from the curve B in Fig. 13 when terminal velocity approaches zero. Furthermore, curve B seems to agree well with impact test data points. However, for higher impact velocities (greater than 110 m/s), curve B slightly deviates from the impact test results. This is because the assumed extended damaged zones may not be very close to the test result. Nevertheless, an examination of curve B in Fig. 13, where the simulated residual velocity is near zero, leads one to conclude that the predicted ballistic limit for two-step braided composites is closer to that found in impact test measurement results. The average ballistic limit shown in Table 5 seems to overestimate test-determined ballistic limit. This is due to the enlargement of the major fiber broken damage area that occurs as the incident velocity is increased.

The purpose of this paper is to report a simple and effective method to predict the ballistic limit of the two-step braided textile composites struck by a hemispherical tip-ended rigid projectile numerically, without performing a series of expensive impact tests. Further study to determine a more sophisticated strain- or stress-state based damage criterion for finite element analysis seems important for prediction of the impact response of targets with varying penetrator diameter and/or target span-to-thickness ratio.

V. Conclusion

The ballistic impact response of three-dmensional two-step braided textile composite plates struck by a hemispherical rigid projectile is studied here. A series of quasistatic punch tests were conducted to investigate the progressive damage modes of the target, to obtain the punch load-displacement relationship, and to characterize the penetration process to be used in the dynamic analysis. After specimens were perforated, a steady friction force was observed in the quasistatic punch tests. A pneumatic launcher was used to propel the projectile with incident velocities ranging from 70 to 170 m/s. The ballistic limit was experimentally determined and the corresponding impact damage pattern was also reported. As was the case in punch test results, the major damage modes of impacted specimens were found to be indentation, matrix failure, and fiber breakage with axial and braider fiber yarn pullout. When the projectile incident velocity is in the range of 70–110 m/s, the impact-induced target damage pattern and area are similar to those observed in the quasistatic punch test results. However, if incident velocity is higher than approximately 110 m/s, the damaged area and the region of fiber pullout are further enlarged. Commercial finite element code (MARC) was incorporated with a constitutive relationship for two-step braided composites (consisting of three unit cells) and the proposed static penetration model to simulate the dynamic impact response. An energy consideration was applied to predict the projectile residual velocity and ballistic limit. Because of the rate dependency nature of glass fiber reinforced plastics composites, both static and dynamic elastic properties were used to examine the strain-rate effect on the predicted dynamic impact response numerically. Numerically simulated results based on the static elastic properties of targets seem to overestimate the projectile exit velocities. When the target's elastic moduli used in simulation are increased by 1.5 times the static values, good agreement between the simulated terminal velocities and the test results is found for projectile incident velocities ranging from 70 to 180 m/s.

Acknowledgments

The authors would like to thank the National Science Council, Republic of China, for funding this research under Contract NSC84-2212-E006-059 and T. W. Chou for his assistance on developing the three-dimensional elastic constitutive relationship for predicting the ballistic limit of the two-step braided composites.

References

[1]Greszczuk, L. B., "Damage in Composite Materials Due to Low Velocity Impact," *Impact Dynamics*, edited by J. A. Zukas, T. Nicholas, H. F. Swift, L. B. Greszczuk, and D. R. Curran, Wiley, New York, 1982, pp. 55–94.

[2]Chou, T. W., *Microstructural Design of Fiber Composites*, Cambridge Univ. Press, Cambridge, England, UK, 1992.

[3]Byun, J. H., and Chou, T. W., "Modeling and Characterization of Textile Structural Composites: A Review," *Journal of Strain Analysis*, Vol. 24, No. 4, 1989, pp. 65–74.

[4]Ko, F. K., "Tensile Strength and Modulus of a Three-Dimensional Braided Composite," *Composite Materials: Testing and Design*, American Society for Testing and Materials, STP 893, North Wales, PA, 1986, pp. 392–403.

[5]Ma, C.-L., Yang, J.-M., and Chou, T. W., "Elastic Stiffness of Three-Dimensional Braided Textile Structural Composites," *Composite Materials: Testing and Design*, American Society for Testing and Materials, STP 893, North Wales, PA, 1986, pp. 404–421.

[6]Ko, F. K., and Hartman, D., "Impact Behavior of 2-D and 3-D Glass/Epoxy Composites," *SAMPE Journal*, Vol. 22, July/Aug. 1986, pp. 259–266.

[7]Gong, J. C., and Sankar, B. V., "Impact Properties of Three-Dimensional Braided Graphite/Epoxy Composites," *Journal of Composite Materials*, Vol. 25, June 1991, pp. 715–731.

[8]Zuksa, J. A., "Penetration and Perforation of Solids," *Impact Dynamics*, edited by J. A. Zukas, T. Nicholas, H. F. Swift, L. B. Greszczuk, and D. R. Curran, Wiley, New York, 1982, pp. 170–174.

[9]Cantwell, W. J., and Morton, J., "Impact Perforation of Carbon Fibre Reinforced Plastics," *Composite Science and Technology*, Vol. 38, No. 2, 1990, pp. 119–141.

[10]Zhu, G., Goldsmith, W., and Dharan, C. K. H., "Penetration of Laminated Kevlar by Projectiles—II. Analytical Model," *International Journal of Solids Structures*, Vol. 29, No. 4, 1992, 421–436.

[11]Lee, S.-W. R., and Sun, C. T., "Modeling of Penetration Process for Composite Laminates Subjected to a Blunt-Ended Punch," *Proceedings of the 23rd International SAMPE Technical Conference* (Kiamesha Lake, NY), 1991, pp. 624–638.

[12]Lee, S.-W. R., and Sun, C. T., "Ballistic Limit of Composite Laminates by a Quasi-Static Penetration Model," *Proceedings of the 24th International SAMPE Technical Conference* (Toronto, ON, Canada), 1992, pp. T497–T511.

[13]Jenq, S. T., Jing, H.-S., and Chung, C., "Predicting the Ballistic Limit for Plain Woven Glass/Epoxy Composite Laminate," *International Journal of Impact Engineering*, Vol. 15, 1994, pp. 451–464.

[14]Du, G. W., Choi, T. W., and Propper, P., "Analysis of Three-Dimensional Textile Preforms and Multidirectional Reinforcement of Composites," *Journal of Material Science*, Vol. 26, 1991, pp. 3438–3448.

[15]Chou, T. W., private communication, Univ. of Delaware, 1994.

[16]Yang, S. H., and Sun, C. T., "Indentation Law for Composite Laminates," American Society for Testing and Materials, STP 787, North Wales, PA, pp. 425–449.

[17]Jenq, S. T., and Sheu, S. L., "High Strain Rate Compressional Behavior of Stitched and Unstitched Composite Laminates with Radial Constraint," *Composite Structures*, Vol. 25, Nos. 1–4, 1994, pp. 427–438.

[18]Harding, J., and Welsh, L. M., "A Tensile Testing Technique for Fiber-Reinforced Composites at Impact Rates of Strain," *Journal of Material Science*, Vol. 18, 1983, pp. 1810–1826.

[19]Kawata, K., Hashimoto, S., Sekino, S., and Takeda, N., "Macro- and Micro-Mechanics of High-Velocity Brittleness and High-Velocity Ductility of Solids," *Proceedings of the IUTAM on Macro- and Micro-Mechanics of High Velocity Deformation and Fracture (MMMHVDF)* (Tokyo, Japan), Springer–Verlag, Berlin, 1985, pp. 91–112.

[20]Mo, J. J., "Ballistic Impact Response of 3-D Braided Glass/Epoxy Textile Composite," M.S. Thesis, National Cheng Kung Univ., Tainan, Taiwan, ROC, 1994.

[21]Goldsmith, W., *Impact*, Edward Arnold, London, 1960.